Progress in Aerospace Sciences 47 (2011) 621–635

Contents lists available at SciVerse ScienceDirect

Progress in Aerospace Sciences

journal homepage: www.elsevier.com/locate/paerosci

NeoCASS: An integrated tool for structural sizing, aeroelastic analysis and MDO at conceptual design level

Luca Cavagna, Sergio Ricci *, Lorenzo Travaglini

Dipartimento di Ingegneria Aerospaziale, Politecnico di Milano, Italy

ARTICLE INFO

Available online 29 September 2011

Keywords:
Aeroelasticity
Conceptual design
Multi-disciplinary optimization
Computational fluid dynamics

ABSTRACT

This paper presents a design framework called NeoCASS (Next generation Conceptual Aero-Structural Sizing Suite), developed at the Department of Aerospace Engineering of Politecnico di Milano in the frame of SimSAC (Simulating Aircraft Stability And Control Characteristics for Use in Conceptual Design) project, funded by EU in the context of 6th Framework Program. It enables the creation of efficient low-order, medium fidelity models particularly suitable for structural sizing, aeroelastic analysis and optimization at the conceptual design level.

The whole methodology is based on the integration of geometry construction, aerodynamic and structural analysis codes that combine depictive, computational, analytical, and semi-empirical methods, validated in an aircraft design environment.

The work here presented aims at including the airframe and its effect from the very beginning of the conceptual design. This aspect is usually not considered in this early phase. In most cases, very simplified formulas and datasheets are adopted, which implies a low level of detail and a poor accuracy. Through NeoCASS, a preliminar distribution of stiffness and inertias can be determined, given the initial layout. The adoption of empirical formulas is reduced to the minimum in favor of simple numerical methods. This allows to consider the aeroelastic behavior and performances, as well, improving the accuracy of the design tools during the iterative steps and lowering the development costs and reducing the time to market.

The result achieved is a design tool based on computational methods for the aero-structural analysis and Multi-Disciplinary Optimization (MDO) of aircraft layouts at the conceptual design stage. A complete case study regarding the TransoniCRuiser aircraft, including validation of the results obtained using industrial standard tools like MSC/NASTRAN and a CFD (Computational Fluid Dynamics) code, is reported. As it will be shown, it is possible to improve the degree of fidelity of the conceptual design process by including tailored numerical tools, overcoming the lacks of statistical methods. The result is a method minimally dependent on datasheets, featuring a good compromise between accuracy and costs.

Contents

1. Introduction . . . 622
2. Layout of NeoCASS . . . 622
3. Initial structural sizing using GUESS . . . 623
4. Aeroelastic analysis using SMARTCAD . . . 624
   4.1. Optimization module . . . 624
5. Interfacing NeoCASS with medium fidelity tools based on CFD . . . 625
6. Application of NeoCASS to a transonic cruiser: a case study . . . 625
   6.1. Geometry description . . . 625
   6.2. Weight and balance results . . . 626

* Corresponding author.
E-mail address: sergio.ricci@polimi.it (S. Ricci).

0376-0421/$ - see front matter © 2011 Elsevier Ltd. All rights reserved.
doi:10.1016/j.paerosci.2011.08.006

6.3. First structural sizing results obtained using GUESS . . . 627
6.4. Aeroelastic analysis using SMARTCAD: frozen maneuvers . . . 628
6.5. Rigid and deformable stability derivatives . . . 629
7. SMARTCAD validation using low, medium fidelity CFD-based tools and wind tunnel testing . . . 629
7.1. CFD aerodynamic model and comparisons . . . 630
7.2. Trim analysis . . . 631
7.2.1. Aeroelastic derivatives . . . 632
8. Conclusions . . . 634
Acknowledgements . . . 634
References . . . 634

1. Introduction

Most of the life-cycle cost of an aircraft is incurred during the conceptual design phase and therefore, the earlier an appropriate conceptual configuration can be found, the more economical the whole design process will be, avoiding costly later redesign and corrections. Contemporary commercial aircraft conceptual design tools make extensive use of handbook methods based on semi-empirical theory and data. In particular, during the conceptual design phase, statistical-based approaches are adopted for structural weight estimation, like those reported in Refs. [1,2]. Nevertheless, it appears as rather unreliable to adopt statistical-based approaches where knowledge is not sufficiently available, e.g. unconventional configurations and new technologies such as Joined Wings [3,4] and Blended Wing Body aircraft [5]. The use of statistics for the structural weight estimation implies that almost all airframe information are practically absent till the preliminary design phase. Due to this choice, it is almost impossible to include aeroelastic requirements that in fact are considered later during the design loop.

As a matter of fact, new transport aircraft are very flexible and aeroelastic effects must be tackled right from the beginning of the design phase, avoiding expensive redesign during preliminary design phase and weight penalties needed to satisfy aeroelastic requirements not previously taken into account. Recently, new software systems specifically tailored for aircraft conceptual design have been proposed (see Ref. [6]). They are composed by specific modules encompassing different aspects and requirements, such as those coming from environmental impact. However, the capabilities of considering more realistic structural models are still missing. In some cases, statistical-based approaches for the prediction of the structural weight are simply overcome by a single loading parameter, like the root wing bending moment. Specific methods based on semi-analytical approaches have then been developed to have a realistic overview of the airframe [7,8]. However, in many cases they are specific modules not included into a more general aircraft conceptual design framework, where aircraft performances and stability and control can be evaluated for example.

The need for aeroelastic analysis capability within SimSAC project has led to the development of a completely new specialized module called NeoCASS (Next Generation Conceptual Aero-Structural Sizing Suite) to perform structural sizing, aeroelastic analysis and optimization within the conceptual design process.

The following pages give a detailed description of NeoCASS and each of its modules.

2. Layout of NeoCASS

NeoCASS (*Next generation Conceptual Aero Structural Sizing*) is a suite of modules that combines state of the art computational, analytical and semi-empirical methods to tackle all the aspects of the aero-structural analysis of a design layout at conceptual design stage. It gives a global understanding of the problem at hand without neglecting any aspect of it: weight estimation, initial structural sizing, aerodynamic performances, structural and aeroelastic analysis from low to high speed regimes, divergence, flutter analysis and determination of trimmed condition and stability derivatives both for the rigid and deformable aircraft.

NeoCASS includes two main modules, named GUESS (*Generic Unknowns Estimator in Structural Sizing*) and SMARTCAD (*Simplified Models for Aeroelasticity in Conceptual Aircraft Design*), respectively. A connection to a third module, called W&B (*Weight and Balance*), shared by other programs available in SimSAC, is also available.

Fig. 1 outlines the different pieces involved. AcBuilder is used to define the general external and internal layout of the aircraft interactively and easily, thanks to a user-friendly graphical interface. Some examples are given in Fig. 2.

When the CFD solver Edge developed by FOI is used for higher fidelity simulations, vibration modes are given by SMARTCAD to carry out Fluid and Structure Interaction (FSI) simulations, such as static or dynamic coupled response, using the built-in functionalities. Also, the aero database for the Flight Control System (FCS) software can be enhanced with the effects of flexibility on stability derivatives through correction coefficients for the rigid values. In order to start the aeroelastic analysis, the semi-analytical module GUESS, based on a modified version of the AFaWWE code (*Analytical Fuselage and Wing Weight Estimation*) [9], is run to produce a first-try stiffness distribution. The sizing is performed in a fully stressed design condition. Formulas from experimental surveys are adopted to include instability limits related to compressed panels and stiffeners (see Section 3). See Ref. [10] for further information. During this first sizing phase, no aeroelastic effect is considered. After the initial structural sizing is completed and the first stiffness distribution is determined,

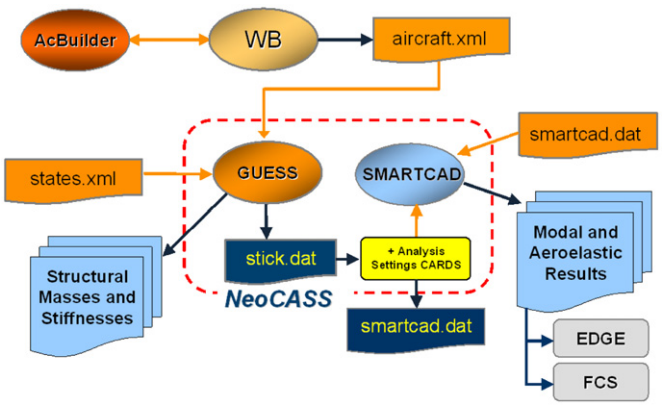

Fig. 1. NeoCASS layout.

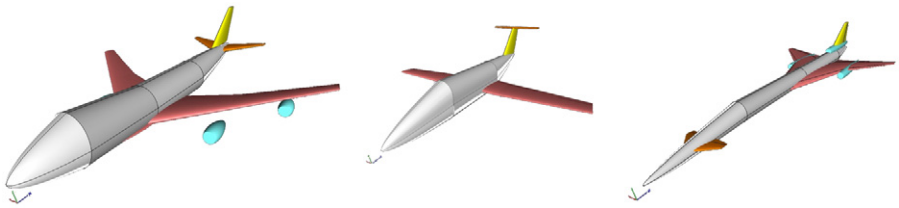

Fig. 2. Samples of parametric geometry models.

GUESS automatically generates the structural and aerodynamic mesh for the numeric aeroelastic assessment by means the dedicated module SMARTCAD. A dedicated Multi-Disciplinary Optimization (MDO) tool is also available in NeoCASS, so that the initial structural sizing can be efficiently refined in order to satisfy the aeroelastic constraints, e.g. divergence speed, aerodynamic derivatives with aeroelastic corrections, maximum deformed shape under loading due to structural flexibility, flutter speed. The aircraft external geometry is kept as fixed; the structural parameters are the only design variables used during this process. By including an MDO module, it is possible to consider specific aeroelastic requirements that cannot be taken into account during the first initial estimation of the stiffness distribution, being the problem implicit. An application to the flutter problem is given in Ref. [11].

3. Initial structural sizing using GUESS

A method based on fundamental structural principles for estimating the load-bearing airframe for fuselage and lifting surfaces is adopted for GUESS module. This method is particularly useful for the weight estimation of aircraft at conceptual level since it represents a compromise between the rapid assessment of component weight using empirical methods, based on actual weights of existing aircraft and detailed but time-consuming finite-element analysis. The present work starts from the work originally performed by Ardema [9], further extended to the sizing of horizontal and vertical tail planes so that a complete view of the whole airframe is given. The distribution of loads and vehicle geometry is accounted for, since the analysis is done station-by-station along the vehicle longitudinal axis and along each lifting surface axis, giving an integrated weight which depends on the local load condition and on the structural concept adopted.

A concept is a pre-defined shape of section for both the wing box and the fuselage. Different parameters for the covers and webs concurring to its stiffness and inertia are defined. The values of the parameters are determined through principles of minimum weight during the sizing phase once the resultants on the each section are available. The reader is referred to Ref. [10] for further information.

Finite-element methods, commonly used in more detailed phases, are not appropriate for the conceptual design, as the idealized structure model must be built off-line and many details are missing in such a premature phase. The following two approaches which may simplify the finite-element model also have drawbacks. The first aims at creating detailed analysis models in correspondence of few critical locations on the fuselage and wing, to successively extrapolate the results to the entire aircraft. This approach can be misleading because of the great variety of structural, load and geometric characteristics in a typical design.

The second approach aims instead to creating a coarse model of the aircraft, but this scheme may miss key loading and stress concentrations.

Two are the strategies implemented in GUESS. They are considered as a good starting point considering the early design phase.

GUESS is said to be in Standard Mode (GUESS SM) when predefined basic maneuvers are used as sizing conditions. The standard maneuvers are pull-up at prescribed normal load, landing, bump on irregular runway, and rudder maximum deflection. The limits depend on the design specifications (for example maximum load factor, landing sink velocity, differential pressure inside the fuselage). Specific lateral maneuvers according to FAR-25 criteria are also considered to improve the accuracy of vertical tail sizing, i.e. abrupt rudder maneuvers and engine-out sideslip flight. To estimate some of the key lateral directional analysis, including stability and control derivatives for use in estimating aircraft characteristics, the approach proposed by Mason [12] is adopted.

On the other hand, GUESS is said to be in Modified Mode (GUESS MM) when the designer can specify a generic maneuver through a consistent definition of the complete state vector and choice of the unknowns of the trim problem. Any kind of symmetric and asymmetric maneuvers can be used without any limitation.

Once the loads are defined by GUESS SM or MM, the sizing is performed for each station under the constraints of ultimate compressive and tensile strength, local and global buckling and minimum gage. Principles of minimum weight are used such that, given an applied load and the limitations on the outside dimensions, the most efficient type of construction, its geometry and material are directly determined [13,14,9]. As mentioned before, at the end of the sizing process, GUESS automatically generates a stick beam model for SMARTCAD. All the parameters of the section like skin, frames, and spar thickness concur to the definition of its stiffness. A semi-monocoque method is used in this respect. Fig. 3 shows some details of the typical model generated. Besides exporting the basic stick model and its mechanical properties, extra information are given:

- stress-recovery points along the sides of the wing-box and fuselage where stresses are evaluated;
- extra-nodes perpendicular to the beam axis and rigidly connected to beam nodes (hypothesis of beam model implying rigid section); they immediately enable to visualize the twist rotational motion of the boundaries of the wing-box and are used as extra set of information for the spatial coupling with the aerodynamic model to transfer forces and displacements along the boundaries.

During the creation of the beam stick model, all non-structural masses are correctly introduced in the structural mesh. Lumped non-structural masses, e.g. engines, landing gears, auxiliary tanks, systems, are directly positioned along the corresponding nodes of the mesh. Non-structural densities per unit length are included to consider passengers in fuselage, fuel in wings, paint, furniture; every corresponding beam features a constant non-structural density along its axis.

The aerodynamic mesh created can be used for classic lifting surface panel methods such as the Vortex Lattice [15], Vortex

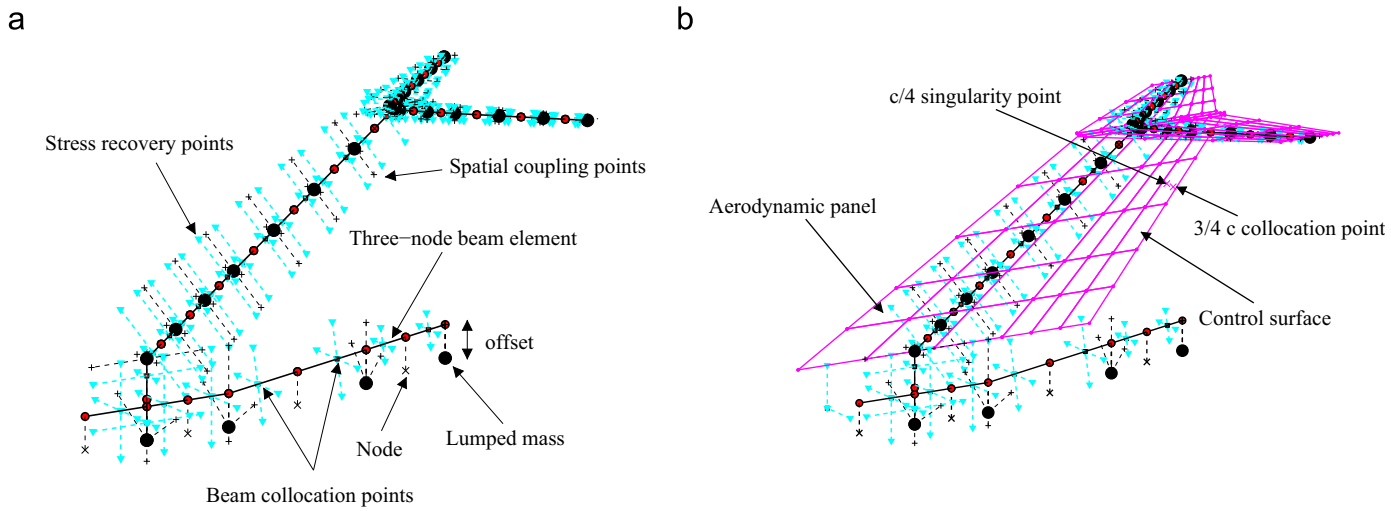

Fig. 3. Nomenclature for the aeroelastic model: (a) structural model and (b) structural and aerodynamic coupled models.

Ring [16], Doublet Lattice [17] and Harmonic Gradient [18]. The aerodynamic shape is represented by a series of two-dimensional trapezoidal surfaces. In some cases the aerodynamic built-in twist can be included as well. Airfoils are defined at different spanwise control sections. This allows to determine the dimensions of the wing-box and consequently the allowable internal volume for fuel. Also, the camber mean line can be used to correctly apply no-penetration boundary conditions.

Finally, considering the early design phase the framework is intended for, control surfaces are currently represented by their aerodynamic contribution only, neglecting their inertia, dynamics and actuation systems. This is postponed to later phases of the project.

4. Aeroelastic analysis using SMARTCAD

Inside NeoCASS, SMARTCAD is the module dedicated to the numerical aero-structural analysis. It can be used as a stand-alone application once the structural and aerodynamic meshes are provided by GUESS, or it can automatically be called by GUESS MM during the sizing process as explained above.

Different kind of analysis can be carried out:

- static analysis, linear buckling;
- vibration modes calculations;
- linearized flutter analysis;
- linear/non-linear static aeroelastic analysis, trimmed calculation for a free-flying rigid or deformable aircraft;
- steady and unsteady aerodynamic analysis to extract derivatives for flight mechanics applications;
- structural optimization.

Besides the aero-structural mesh, specific parameters are usually required to rule the solver, e.g. number of vibration modes, external forces, flight condition, design variables, objective function.

Currently the structural model is represented by a three-node linear/non-linear finite-volume beam element [19]. As mentioned, classic lifting aerodynamic surfaces are used. Two class of methods are available for the spatial coupling between structural and aerodynamic meshes: an innovative scheme, based on Moving Least Square (MLS) method [20] and the Radial Basis Function (RBF) method [21]. Both methods ensure the conservation energy transfer between the fluid and the structure. Also, they are suitable for the treatment of complex configurations because they require a limited amount of information which do not consider mesh connectivity and topology. To avoid interpolating rotations and using the same algorithms in a straightforward way also for CFD meshes, extra points are added along the wingbox through rigid-arms. In this way it is easy to reconstruct the deflections along the aerodynamic surface by finite-differences, avoiding interpolation rotational degrees of freedom. Aerodynamic loads are distributed along both original master beam nodes and these additional nodes. Loads are then reduced to lumped forces and moments on the former set of nodes only which represent the only source of degrees of freedom in the structural problem.

4.1. Optimization module

The first structural sizing on minimum weight principles according to strength criteria on ultimate loads, obtained using GUESS, can be considered to be a good starting point for the distribution of stiffness and inertias. Whether the aeroelastic analysis turns out to be unsatisfactory with respect to some defined parameters, e.g. excessive deformability, loss of efficiency in aerodynamic performances, flutter, the need for a structural optimization arises. In this respect, a simple optimization process can be adopted to adjust the airframe so that aeroelastic requirements are sufficiently satisfied.

The classic statement for the problem of constrained optimization reads:

$$\begin{aligned} &\text{minimize}: \quad I(d_j) \\ &\text{with respect to}: \quad d_j, \quad j=1,2,\ldots,N_d \\ &\text{subject to}: \quad g_m(d_j)\geq 0, \quad m=1,2,\ldots,N_g \end{aligned} \tag{1}$$

where I is a non-linear function of the design variables d_j and g_m are the non-linear constraints to be satisfied.

The parameters are allowed to vary such that the design features at its best the figure of merit I. A typical function considered is the overall structural weight. The design space given by d_j is limited to guarantee a feasible and realistic solution. They may represent the thickness of the skin and spars, the spacing of the frames along the fuselage (see Ref. [9] for more details). Typically, the constraints are of structural and aeroelastic nature. For the former set, g_m may represent the local value of stress g_{m_s} with respect to a safety value $\hat{g}_{m_s}$:

$$\hat{g}_{m_s} - g_{m_s} \geq 0$$

As for the latter, the ratio of typical aerodynamic derivatives for the elastic and rigid case are considered. For example, a limited

decrease for the vertical force coefficient CN with respect to the angle of attack α can be stated as:

$$\frac{(\partial CN/\partial\alpha)_E}{(\partial CN/\partial\alpha)_R} - \hat{\eta} \geq 0$$

where $\hat{\eta}$ is the allowed ratio limit.

Optimization algorithms perform the task given by Eq. (1) in a rigorous way. Many methods are available and the literature on this topic is large, see for example [22]. A well known class is the one based on gradient which uses the value of the objective function and its gradients with respect to the design variables; the sensitivity information is used to determine iteratively the new design variables.

In the present work, the Feasible Direction Method has been adopted together with a simplification based on the convex linearization technique. Indeed, during the optimization process, the objective and the constraints have to be repeatedly evaluated, raising the overall computational cost since each evaluation demands for a numerical simulation. In this respect, a common approach consists in creating an approximated linearized problem for the objective function and constraints and feed the optimizer with such simplified model.

5. Interfacing NeoCASS with medium fidelity tools based on CFD

The strategy adopted inside SimSAC project and during the development of NeoCASS module has been based on the concept of multi-fidelity aerodynamic modeling, as follows:

- Tier 1 tools, adopting VLM/DLM solvers for steady and unsteady aerodynamic calculations. The former has been derived from an available code (Tornado from KTH) while the latter has been developed from scratch. Both tools are completely embedded in NeoCASS and are used during the initial conceptual design phase;
- Enhanced Tier 1 tools, based on FOI-Edge URANS code. In this case the CFD solver is not embedded but data are imported/exported between the two codes running independently.

Once vibration modes are available from NeoCASS, the CFD code allows the creation of a Reduced Order Model (ROM) for the generalized aerodynamic forces. The ROM can then be used by NeoCASS to correct aerodynamic derivatives with deformability effects or to assess flutter run solving for a non-canonic eigenvalues problem. The approach is similar to the one presented in Ref. [23]. The modal model can also be used by Edge to determine a free-flight trimmed condition for the deformable aircraft. Further information can be found in Ref. [24]. Inviscid analysis are usually carried out by means of the transpiration wall boundary condition. This guarantees a good trade-off between accuracy in the transonic regime and the computational costs which must be kept as low as possible due to the large number of configurations to be analyzed during the global optimization loop. Also, the issues related to grid deformation and element distortion, which can dangerously stop the CFD solver in cases of grid invalidations, are avoided.

6. Application of NeoCASS to a transonic cruiser: a case study

The whole procedure here presented has been applied to the conceptual design of a target aircraft depicted in Fig. 5: the TransCruiseR (TCR), most of the work packages in the SimSAC project are focusing in. The aircraft is not existing; it is a test-case proposed by SimSAC to highlight the difficulties in using handbook methodology when designing aircraft operating in the transonic speed region. In particular, the goal is to compare the results gained by means of classic methodologies and the new tools such as NeoCASS developed during the project, once the mission specifications are given and the first sketch and design has to begin. Fig. 4 and Table 1 briefly summarize the main features for the TCR.

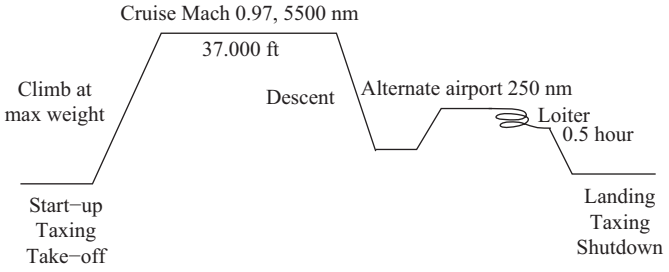

Fig. 4. Mission profile for TCR.

Table 1
Design specifications for TCR.

Cruise Mach	0.97 at altitude $\geq 37,000$ ft
Range	5500 nm + 250 nm to alternate airport 0.5 h loiter at 1500 ft
Max payload	22,000 Kg
Passengers	200
Crew	2 pilots, 6 cabin attendants
Take-off distance	2700 m at max W_{TO} altitude 2000 ft
Landing distance	2000 m at max W_L Altitude 2000 ft max payload and normal reserves
Powerplant	2 turbofans
Certification	JAR25
Maneuvering load factors	2.5, −1
Max load factors	3.1, −1.7

6.1. Geometry description

The layout is defined using the module AcBuilder. Besides the external shape (see Fig. 5(a)), the designer can interactively visualize on the screen the fuel distribution (Fig. 5(b)), baggage and passengers positions (Fig. 5(c)) and the location of the spars along the lifting surfaces (Fig. 5(d)). Concerning the external geometry, different assumptions have been introduced. As reported in Table 2(a), three trapezoidal patches compose the wing. Each of them is defined by inboard and outboard chords c_1, c_2, span b, leading edge sweep λ_{LE}, dihedral Λ inboard and outboard twist angles α_1, α_2. For the canard and the fin (Table 3(a) and (b)), two patches are used. The fuselage features a cone for the nose, two cylinders (the first with the diameter linearly varying along the axis, the second with a constant diameter) and a final cone for the tail. Each trunk has an initial and final diameter d_1, d_2, length l and axis orientation ω with respect to the fuselage mean line. Table 4 reports the apex position for all aerodynamic surfaces with respect to the fuselage nose ($\mathbf{x}$) and the symmetry plane ($\mathbf{y}$ and $\mathbf{z}$). The reference system is depicted in Fig. 5(a). To completely define the aerodynamic geometry, data about control surfaces are required. The wing has three movable surfaces, one for each trapezoidal section: two independent flaps, covering the 20% of local chord, one aileron on the outboard section starting at a spanwise position of $\mathbf{y}=15$ m and covering the 25% of local chord. The main surface for pitch control is represented by the canard that is all movable and has a hinge axis at 50% of local chord. The fore spar of canard is at the 15% of local chord, while the aft one at the 65%. Lateral control is guaranteed

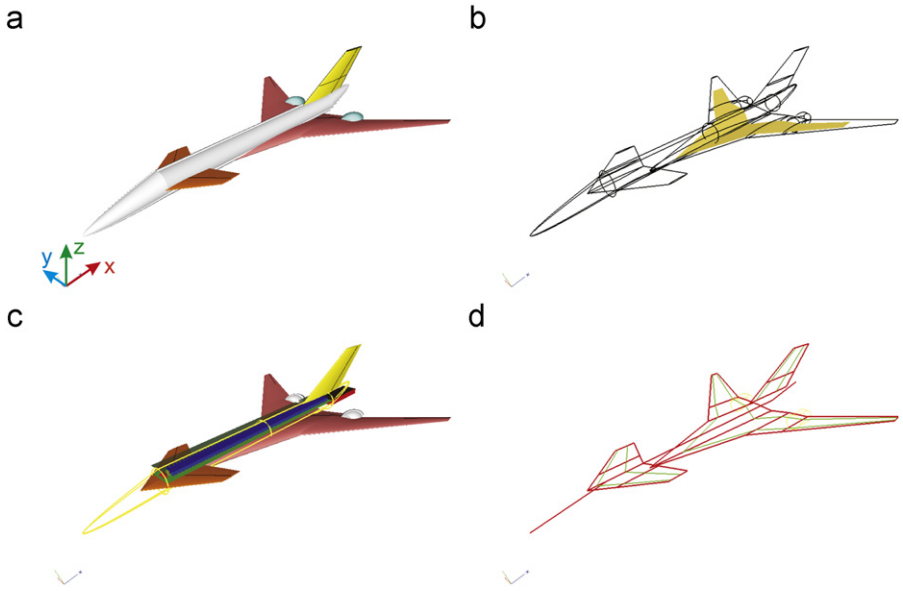

Fig. 5. Few screenshots from AcBuilder: (a) geometry, (b) fuel distribution, (c) passengers and baggage and (d) Spar location.

Table 2
Geometry data for wing and fuselage.

Property	In	Mid	Out
(a) Wing			
c_1 (m)	33.52	15.28	10.03
c_2 (m)	15.28	10.03	2.45
b (m)	4.36	4.14	13.82
λ_{LE} (degree)	76	50	50
Λ (degree)	3	3	3
α_1 (degree)	1	1	1
α_2 (degree)	1	1	−1
	Nose	**Aft**	**Fore**	**Tail**
(b) Fuselage				
d_1 (m)	0	3.7	3.7	3.7
d_2 (m)	3.7	3.7	3.7	0
l (m)	10	20	20	10
ω (degree)	30	0	0	−15

Table 3
Geometry data for the canard and vertical fin.

Property	In	Out
(a) Canard		
c_1 (m)	7	6.77
c_2 (m)	6.77	3.43
b (m)	2.1	3.9
λ_{LE} (degree)	53	53
Λ (degree)	0	0
α_1 (degree)	0	0
α_2 (degree)	0	0
(b) Fin		
c_1 (m)	13.96	11.51
c_2 (m)	11.51	6.98
b (m)	2.86	5.32
λ_{LE} (degree)	62.03	62.03
Λ (degree)	0	0
α_1 (degree)	0	0
α_2 (degree)	0	0

by one rudder covering all the span of the fin with the 30% of the local chord. The fore spar is at the 15% of local chord, while the aft at the 70%.

Table 4
Aerodynamic surface positions.

Component	**x** (m)	**y** (m)	**z** (m)
Wing	16.8	0	−1.258
Canard	7.2	0	0
Fin	41.46	0	1.85

Table 5
TCR weight survey.

Component	Mass (kg)
Wing	23.764
Canard	764
Vertical tail	955
Landing gear	6.352
Fuselage	18.623

To conclude the outline of the TCR, few information for the payload are given. The fuel is distributed along the wing and part of the central fuselage. Wing tanks are delimited by the fore spar at the 15% of local chord, and by the aft spar at the 75% of local chord, from the root up to the 70% of the span The configuration considered through all the work is the one with maximum passengers (200) uniformly distributed along the two central cylindrical sections. Baggages are located in the tail fuselage cone only.

6.2. Weight and balance results

The W&B module is applied to the TCR jet transport introduced above, given its layout and its design specifications in terms of maximum payload as input.

Starting from an estimation of a total fuel amount of 106,186 kg, distributed between wing and central-fuselage tanks, the predicted Maximum Take-Off Weight (MTOW) is 193,672 kg, while the Maximum Empty Weight (MEW) is 69,093 kg. A brief survey of the main weights for the different components is reported in Table 5. The values refer only to the structural contribution, being the focus of the present work.

Non-structural masses, such as systems, furniture and interior, are estimated separately when they are not directly given by the designer. Of course they contribute to the total weight of each component, i.e. wing, tail, fuselage. For example, the final weight for the fuselage is given by the sum of the value reported in the table and 17,966 kg which is derived from statistics to represent the furniture and the interior.

Finally, Table 6 reports the estimated position of the center of gravity along the longitudinal axis for both configurations (the length of the fuselage is 60 m) and the principal moment of inertia at MTOW. Again, statistics are used to recover all the information.

These values will be then used in the structural sizing process for the determination of inertial loads. When the mesh is exported, the weight and balance is recovered from the numerical model which now considers the real load bearing material distribution. Thus the values previously determined through statistics are overwritten.

6.3. First structural sizing results obtained using GUESS

The structural sizing has been achieved by using the two strategies available in GUESS, *Standard Mode* (SM) and *Modified Mode* (MM). The first approach recovers sizing-loads due to maneuvers classically defined by regulations, i.e. yawing maneuver conditions due to engine-out, pull-up at a given load factor. The aircraft is simply represented by a point mass, undergoing inertial and aerodynamic loads due to the maneuver considered. Rotational inertias are considered as well. The second approach couples the sizing process performed by GUESS with SMARTCAD which provides the trim solution and the aerodynamic forces. The designer can define a set of frozen maneuvers at his taste. GUESS generates the first aeroelastic model using the standard mode and then refines the first solution applying the loads coming from the numerical analysis. At each step, the inertial and mechanical properties of beam elements are updated and the set of maneuver is run again, until the process converges.

Table 6
TCR inertia survey.

x_{MEW} (m)	x_{MTOW} (m)	I_{xx} (kg m^2)	I_{yy} (kg m^2)	I_{zz} (kg m^2)
36.55	36.6	9502×10^6	2015×10^7	$27,737 \times 10^7$

Table 7
TCR weight and inertia survey.

Code	x_{MTOW} (m)	I_{xx} (kg m^2)	I_{yy} (kg m^2)	I_{zz} (kg m^2)
W&B	36.6	9502×10^6	2015×10^7	$27,737 \times 10^7$
GUESS SM	35.22	$55,465 \times 10^6$	$18,205 \times 10^7$	$23,034 \times 10^7$
GUESS MM	35.72	$54,776 \times 10^6$	$18,224 \times 10^7$	$22,691 \times 10^7$

The following three maneuvers have been defined for the sizing:

1. normal load factor $n_z=3.1$, altitude $z=0$ m, $M_\infty=0.6$;
2. level flight with sideslip angle $\beta=25^\circ$, altitude $z=0$ m, $M_\infty=0.65$;
3. a transition from leveled flight into a snap-roll given abrupt deflection on the canard and the rudder, $z=0$ m, $M_\infty=0.6$, $\delta_c=30^\circ$, $\delta_r=30^\circ$.

A subsonic free-stream Mach number M_∞ has been considered only. After the first structural sizing (Guess SM), the MTOW weight is 215.211 kg. After few iterations with GUESS MM, the value is 223.679 kg. The total weights have been determined considering two regressions on the basis of the load-bearing material which is predicted numerically under physical basis. The regressions are used to determine the weight of secondary items, e.g. junctions, stiffeners, concurring to the final structural weight. The position of the center of gravity for the MTOW configuration and total inertias for both methods are reported in Table 7.

Table 8 compares the results by W&B with the new estimation of the structural components determined by GUESS SM and MM; the weight for the load-bearing material and for the total weight resulting from the two steps of regression are reported as well. The results obtained with GUESS MM and SM are very dissimilar, especially for the vertical tail and the canard. Moreover, both results are very different from the values predicted by W&B. It is interesting to compare for each components (wing Fig. 6(a), fuselage (b), canard (c), vertical tail (d)) the structural mass distribution determined by the two different approaches.

The mass distribution for the sole wing is quite similar while the other items have major discrepancies. As for the fuselage, GUESS SM predicts a maximum in correspondence of the wing root; the peak is higher when GUESS MM is considered. A second local maximum appear at the fuselage-canard intersection, now higher the one from GUESS MM. Thus, GUESS SM and MM distribute the total longitudinal load required to trim the aircraft in a different way between the canard and the wing. This explains the differences found in the load resultants at the intersection between the fuselage and the two lifting surfaces.

Concerning the vertical tail, the sole yawing maneuver condition is not sufficient to size the fin. Fig. 7 gives an overview of the aero-structural mesh created for the aeroelastic and MDO procedures. All the parameters ruling the geometry of the aircraft are available in GUESS which automatically creates the Vortex/Doublet Lattice mesh. Furthermore, since the wing box for the lifting surfaces is completely defined, extra points are added to the numerical model for stress-recovery purposes. They are laid along the mid-side of each side of the wing box section. Finally, all the internal database is transferred to SMARTCAD, i.e. material and beam properties, nodes, connectivities, aerodynamic mesh and control surfaces position. The structural model chosen to conduct all the following analysis is the output from GUESS MM. This model has then been validated comparing the inertial properties and the modal solution with MSC/NASTRAN. Table 9 compares

Table 8
TCR weight survey.

Component	GUESS bearing material [kg]		GUESS primary weight (kg)		GUESS total (kg)		W&B total (kg)
	SM	MM	SM	MM	SM	MM	
Wing	15,506	19,353	21,176	26,429	27,367	34,156	23,764
Canard	2373	899	3240	1228	4188	1587	764
Vertical tail	2268	4756	3097	6496	4003	8395	955
Fuselage	9060	10,849	12,663	15,162	17,235	20,637	18,623

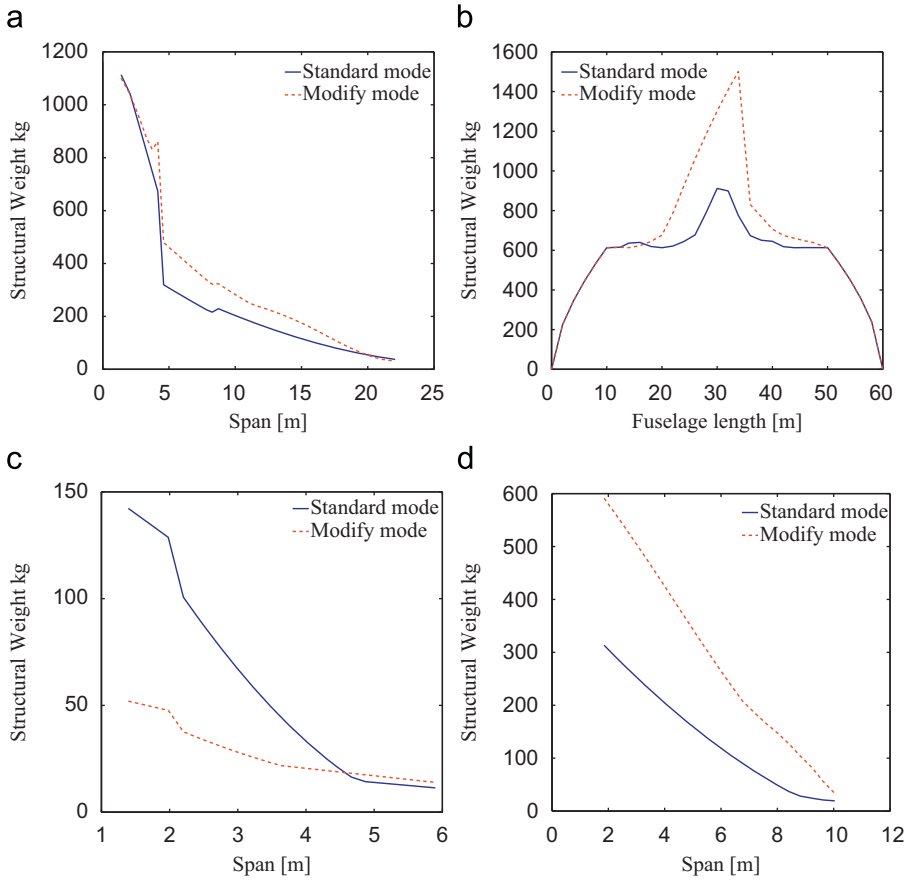

Fig. 6. Mass distribution: (a) wing, (b) fuselage, (c) canard and (d) vertical tail.

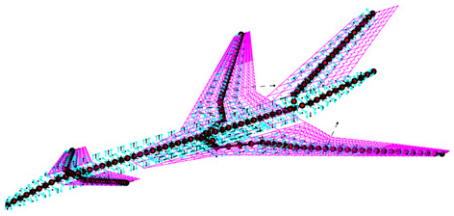

Fig. 7. Aero-structural mesh.

Table 9
Comparison of frequencies (Hz) for the first ten vibration modes.

Code	m 7	m 8	m 9	m 10	m 11	m 12	m 13	m 14	m 15	m 16
NeoCASS	1.85	2.27	2.48	2.69	2.92	3.36	4.18	5.00	5.73	6.44
NASTRAN	1.84	2.28	2.49	2.71	2.94	3.35	4.12	5.03	5.78	6.48

Table 10
Weight and inertia comparison.

Code	x_{MTOW} (m)	MTOW (kg)	I_{xx} (kg m^2)	I_{yy} (kg m^2)	I_{zz} (kg m^2)
Neo	35.72	223,679	$54,776 \times 10^6$	$18,224 \times 10^7$	$22,691 \times 10^7$
NAS	35.71	223,819	$52,862 \times 10^6$	$18,006 \times 10^7$	$22,729 \times 10^7$

the first ten frequencies for the unconstrained model. Table 10 summarizes the main inertial properties. The correlation between the two solvers is quite good.

6.4. Aeroelastic analysis using SMARTCAD: frozen maneuvers

The methodology adopted in SMARTCAD relies on the classic approach used in linear aeroelastic analysis [25] which allows to perform rapid trim calculations for the restrained/unrestrained aircraft and evaluate the corrections to its stability derivatives due to the structural flexibility. At this early phase, the quality of the preliminary sizing is assessed by considering its integrity and the requirements on the maximum static displacements and deflections allowed. The methodology developed allows to compare the solution of the trim to the rigid case, in terms of excessive control deflections to attain the required maneuver, excessive deformability and/or changes in the aerodynamic derivatives, for example.

For the test-case here considered, the following frozen maneuvers have been considered in order to highlight lacks in the initial sizing GUESS process:

1. normal load factor $n_z=3.1$, $z=5000$, $M_\infty=0.6$;
2. a high-speed steady rolling pullout given an aileron input δ_a of 25°, vertical load factor of $n_z=3.1$ (and corresponding pitch rate $q=(-n_z-1)\,g/V_\infty$), $z=5000$ m, $M_\infty=0.6$;
3. cruise flight with sideslip angle $\beta=20°$, $z=5000$ m, $M_\infty=0.6$ and $z=10{,}000$ m, $M_\infty=0.9$;
4. a transition from cruise flight into a snap-roll given an abrupt deflection of the elevator and the rudder, $z=5000$ m, $M_\infty=0.6$ and $z=1000$ m;
5. an abrupt aileron input δ_a of 25° starting from cruise flight, $z=5000$ m, $M_\infty=0.6$.

These conditions have been proposed with the purpose of identifying a good set of loads for each component of the airframe

(fuselage, wing, canard and fin). The maneuvers 1–2 and 3–4 have led to the worst load conditions for wing–canard–fuselage and fin, respectively. The stresses along the wing and fuselage for GUESS SM exceeds the maximum admissible while the solution from GUESS MM features an acceptable safety of margin. Thus, the sole standard load conditions used in GUESS SM may tend to dangerously undersize the structure, in particular in the case of lateral maneuvers. This may lead to a fin structure which is not robust and rigid enough. Fig. 8 shows the trimmed deformed configurations for load cases 1 and 4.

6.5. Rigid and deformable stability derivatives

As already described in the previous paragraphs, the approach adopted for the static aeroelasticity makes the corrections to aerodynamic derivatives with deformable effects straightforward.

Tables 11 and 12 report a comparison between rigid and deformable aerodynamic and control derivatives for a flight Mach number of $M=0.6$. The solutions refer to GUESS SM and MM.

7. SMARTCAD validation using low, medium fidelity CFD-based tools and wind tunnel testing

Low and medium fidelity methods have been applied to the TCR in order to validate the overall analysis tool and to evaluate the enhancements provided by the latter. In this respect, few aspects have been considered: aerodynamic load predictions, trim analysis for the rigid and deformable cases and aerodynamic derivatives evaluation and correction for aeroelastic effects.

As for the validation of the low fidelity tool SMARTCAD, MSC/NASTRAN has been adopted, since it represents a standard 'de facto' for the aerospace industry. Concerning the medium fidelity tool based on the CFD, the code Edge by FOI has been used.

CFD models are used to enhance flow predictions with respect to the classic linear theories of Tier I. Complex flow conditions as well as complex geometries can thus be investigated. On the other hand, such models are computationally demanding and need particular techniques when aeroelastic analysis has to be carry out. Special care has to be taken to reduce the costs and raise the robustness of the algorithms so that this technology can be easily included in the early design process.

In this work, Euler equations have been considered as a good compromise for enhanced flow modeling, mesh requirements and hence overall costs. Compressibility effects can be taken into account, coarser meshes are required and fewer restrictions than Navier–Stokes simulations are demanded. Also, automatic mesh generation for unstructured meshes can be exploited, once a water-tight CAD file is given, allowing to recursively have a new mesh when the external shape of the aircraft is updated during the design loop.

When aeroelastic analysis based on CFD models is considered, the complexity of the whole process is further raised. The flow domain has to be updated to follow the new deformed shape of the aircraft. This demands for special techniques which are both computationally demanding and sometimes lack of sufficient robustness. In this case, this issue overcomes by means of the transpiration method [26]. For inviscid cases and when the structural motion is relatively small, i.e. within the usual linear elastic behavior, the domain need not to be updated; structural effects are simply accounted for as a change in the boundary condition along the physical walls. This also eases the management of control surfaces which have to be deflected when the trim condition for a free flying aircraft is sought.

Table 11
Stability derivatives $M=0.6$.

Derivative	Rigid		Deformable		Deformable/rigid	
	Standard	Modified	Standard	Modified	Standard	Modified
(a) α Derivatives						
C_{L_α}	3.72	3.72	2.86	3.11	0.77	0.84
$C_{\mathcal{M}_\alpha}$	−0.69	−0.69	0.06	−0.22	−0.09	0.31
(b) β Derivatives						
C_{S_β}	0.29	0.29	0.26	0.28	0.88	0.94
$C_{\mathcal{L}_\beta}$	−0.13	−0.13	−0.16	−0.14	1.19	1.05
$C_{\mathcal{N}_\beta}$	0.13	0.13	0.11	0.12	0.87	0.93
(c) p Derivatives						
C_{S_p}	0.03	0.03	0.04	0.04	1.46	1.53
$C_{\mathcal{L}_p}$	−0.49	−0.49	−0.41	−0.43	0.84	0.88
$C_{\mathcal{N}_p}$	−0.01	−0.01	−0.00	−0.00	0.40	0.40
(d) q Derivatives						
C_{L_q}	6.34	6.34	4.81	5.17	0.76	0.82
$C_{\mathcal{M}_q}$	−6.79	−6.79	−5.47	−5.88	0.81	0.87
(e) r Derivatives						
C_{S_r}	−0.37	−0.37	−0.31	−0.34	0.84	0.92
$C_{\mathcal{L}_r}$	0.17	0.17	0.17	0.17	1.00	0.96
$C_{\mathcal{N}_r}$	−0.17	−0.17	− 0.14	−0.16	0.84	0.92

Table 12
Control derivatives $M=0.6$.

Derivative	Rigid		Deformable		D/R	
	Standard	Modified	Standard	Modified	Standard	Modified
(a) $\delta_{aileron}$ derivatives						
$C_{S_{\delta_a}}$	−0.01	−0.01	−0.01	−0.01	1.37	1.55
$C_{\mathcal{L}_{\delta_a}}$	0.10	0.10	0.02	0.06	0.16	0.56
$C_{\mathcal{N}_{\delta_a}}$	−0.00	−0.00	−0.01	−0.01	1.46	1.48
(b) δ_{rudder} derivatives						
$C_{S_{\delta_r}}$	−0.13	−0.13	−0.09	−0.11	0.68	0.83
$C_{\mathcal{L}_{\delta_r}}$	0.02	0.02	0.02	0.02	1.19	1.10
$C_{\mathcal{N}_{\delta_r}}$	−0.07	−0.07	−0.05	−0.06	0.71	0.85
(c) δ_{canard} derivatives						
$C_{L_{\delta_c}}$	0.05	0.05	0.00	0.00	0.05	0.04
$C_{\mathcal{M}_{\delta_c}}$	0.30	0.30	0.34	0.32	1.13	1.05

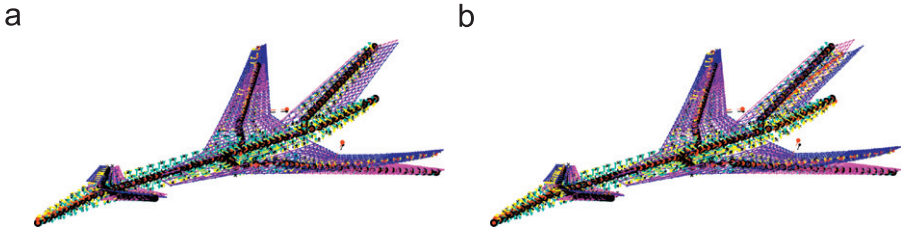

Fig. 8. Deformed model, load condition 1: (a) trim condition 1 and (b) trim condition 4 amplified five times.

For the classic linear aeroelastic analysis, the trim solution is recovered by a matrix of Aerodynamic Influence Coefficients (AIC) giving the relation among the aerodynamic loads, the structural deformation, control surfaces and flight attitude. When non-linear CFD methods are adopted, this is troublesome and an iterative process is usually adopted where boundary conditions are updated, controls are deflected and the effects of structural motion included. To achieve this, a staggered approach has been pursued: an iterative process is carried out which at first determines the flight parameters, e.g. angle of attach and control deflections, to have the aircraft trimmed with a given deformed shape; on a second stage, the new deformed shape is sought with frozen flight parameters by solving the structural equations. The process is iterated until overall convergence is achieved. For simple cases, the aerodynamic derivatives with respect to flight parameters can be efficiently used during the solution of the first task.

Data transfer between the aerodynamic mesh and the structural has to be carried out, so that data, e.g. displacements or forces, are exchanged among the common boundaries. The two methods available in SMARTCAD are used to transfer data with the CFD flow solver: the Moving Least Squares (MLS) technique [20] or Radial Basis Function (RBF) interpolation [21].

Keeping in mind the need to reduce computational costs, a modal approach has been adopted. The creation of a ROM for the aerodynamic generalized forces allows to extract important pieces of information regarding the flow system with few simulations. The ROM can then be used to determine the steady and dynamic aerodynamic derivatives of the aircraft and easily correct them for the aeroelastic effects. Also, flutter can be assessed using the same model [27]. Of course, the vibration modes to be used have to be carefully selected.

Finally, few comparisons between numerical and experimental values for the rigid aircraft have been considered. Indeed, during SimSAC project a 1:40 scale model was designed and manufactured by Politecnico di Milano and tested for steady and unsteady stability derivatives measurement by TsAGI (see Fig. 9).

7.1. CFD aerodynamic model and comparisons

Fig. 10 depicts the two aerodynamic meshes adopted for low and medium fidelity analysis. The main difference relies in how the geometry of the fuselage and its intersection with the lifting surfaces is accounted for. The VLM/DLM mesh represents the fuselage as a simple distribution of flat panels in the plane of the wings only. This allows to maintain the continuity of the aerodynamic load at the root of the lifting surfaces. No longitudinal modeling has been here considered, i.e. the vertical tail has no intersection with the fuselage and all its boundaries are free. However, in the present work only symmetric flight conditions have been considered, making this detail of minor importance with respect to the overall quality of the results. Table 13 reports few details about the two meshes. The VLM/DLM mesh is represented by 18 patches with a total number of 787 panels. The CFD mesh used for inviscid analysis features 178,158 cells and 70,432 surface points along the aircraft surface. The flow solver is indeed based on a node-centered scheme. Despite the latter is not so fine for common CFD application, the differences with the former in terms of surface discretization and in geometric detail modeling are evident. In order to neglect compressibility and viscous effects, a subsonic case at flight Mach number $M_\infty = 0.65$ and null incidence has been considered, resulting in a consistent and fair comparison between the two models.

Table 14 reports the values of the reference normal force coefficient CN_0 and of the pitching moment Cm_0 with respect to the center of gravity. The solutions from the CFD and the VLM models available respectively in SMARTCAD and MSC/NASTRAN are given. For this last, a simple flat model has been considered, i.e. no built-in effects were given by twist or airfoil camber, which explains the null value of force and moment. Edge and

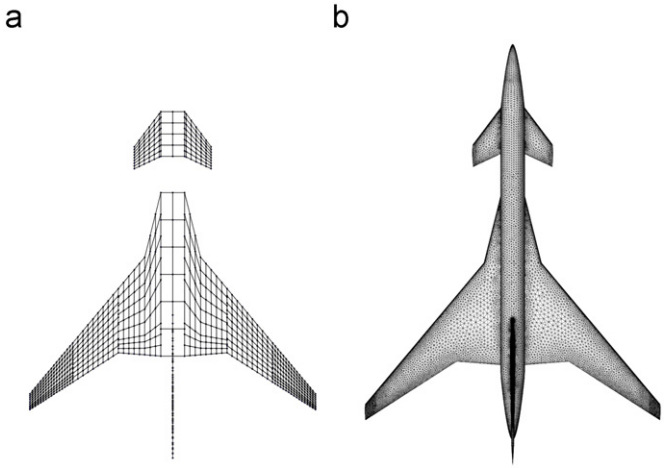

Fig. 10. Meshes adopted in low and medium fidelity analysis (top view): (a) Vortex/Doublet Lattice mesh and (b) CFD mesh (Euler).

Table 13
Distribution of panels for the DLM/VLM and CFD meshes.

Component	VLM/DLM panels	CFD points
Wing	594	45,565
Canard	96	10,335
Fin	77	6526
Fuselage	20	8006

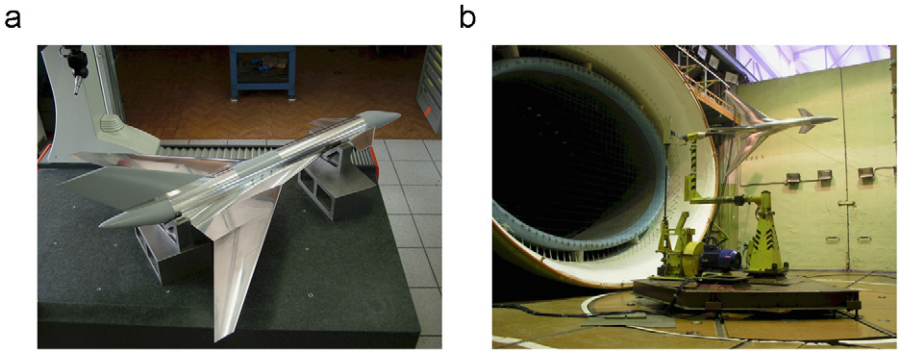

Fig. 9. TCR wind tunnel model: (a) wind tunnel model during final assembling and (b) steady pitch derivatives measurement.

Table 14
Reference values for the leveled flight condition, $\alpha=0^{\circ}$, $M_{\infty}=0.65$, $z=0$ m.

Intercept	Edge	SMARTCAD	MSC/NASTRAN
$\mathbf{CN}_0$	0.14	0.17	0.0
$\mathbf{Cm}_0$	−0.12	−0.09	0.0

Table 15
Longitudinal steady derivatives, $M_{\infty}=0.65$, $z=0$ m, rigid.

Derivative	Edge (FD)	SMARTCAD	MSC/NASTRAN	WT
$\mathbf{CN}_{\alpha}$	3.56	3.92	3.46	3.01
$\mathbf{Cm}_{\alpha}$	−1.25	−0.72	−0.80	−1.00
$\mathbf{CN}_{\delta}$	0.05	0.06	0.06	0.06
$\mathbf{Cm}_{\delta}$	0.44	0.33	0.36	0.40

Table 16
Longitudinal steady derivatives, $M_{\infty}=0.65$, $z=0$ m, rigid.

Derivative	Edge (FD) $\alpha=0$	Edge (ROM) $\alpha=0$	Edge (ROM) $\alpha=\alpha_T$	SMARTCAD	MSC/NASTRAN
$\mathbf{CN}_{\alpha}$	3.56	3.57	3.57	3.92	3.46
$k=0.01$		3.55	3.56		
$\mathbf{Cm}_{\alpha}$	−1.25	−1.29	−1.16	−0.72	−0.80
$k=0.01$		−1.32	−1.22		
$\mathbf{CN}_{\delta}$	0.05	0.04	0.08	0.06	0.06
$\mathbf{Cm}_{\delta}$	0.43	0.45	0.53	0.33	0.36

SMARTCAD predict a pitch down aerodynamic moment, with the former featuring a higher value.

The aerodynamic derivatives for the reference condition have been determined though Finite Difference (FD). For the three different models considered, Table 15 summarizes the longitudinal derivatives of the normal force and pitch moment with respect to the angle of attack α and canard deflection δ. The Wind Tunnel (WT) results are also reported in the last column for comparison. Also the results from the ROM based on CFD at a very low value of the reduced frequency k are reported. They are recovered considering the real or imaginary part of a complex term (see Ref. [28] for further details) being the ROM a function generally speaking of complex frequency.

The larger differences between low and medium fidelity analysis come from the pitching moment derivatives, implying a different pressure load distribution and resultant. Considering the canard for example, the CFD solution results in lower normal force derivative but higher pitching moment, highlighting the importance of local fuselage effects. As mentioned, for the CFD case, the same derivatives have also been determined through a ROM for the rigid body modes at low reduced frequencies for two conditions: $\alpha=0$ and $\alpha=\alpha_T$ which is the angle of attack for the trimmed solution reported in the next section. As shown in Table 16, good agreement between the FD, ROM and wind tunnel testing has been found.

Finally, dynamic derivatives for the rigid aircraft have been considered and reported in Table 17. The results of the ROMs by CFD and the DLM methods available in SMARTCAD and MSC/NASTRAN are compared together with wind tunnel measurements. As expected, the results provided by the enhanced fidelity method are closer to the experiment. Large discrepancies have been determined for the pitching moment derivatives with $\dot{\alpha}$ and q. Again, the contribution of the fuselage is not negligible.

Table 17
Longitudinal dynamic derivatives, $M_{\infty}=0.65$, $z=0$ m, rigid.

Derivative	Edge (ROM) $\alpha=0$	SMARTCAD	MSC/NASTRAN	WT
$\mathbf{CN}_{\dot{\alpha}}$	0.16	−0.63	−0.25	1.25
$\mathbf{CN}_{q}$	−6.22	−5.70	−5.93	−6.34
$\mathbf{CN}_{\dot{\alpha}}+\mathbf{CN}_{q}$	−6.20	−6.34	−6.18	−5.09
$\mathbf{Cm}_{\dot{\alpha}}$	19.19	0.79	1.11	19.00
$\mathbf{Cm}_{q}$	−24.42	−6.64	−4.25	−22.81
$\mathbf{Cm}_{\dot{\alpha}}+\mathbf{Cm}_{q}$	−5.22	−5.85	−5.36	−3.67

Table 18
Trim solution summary.

Trim variables	Edge	SMARTCAD	NASTRAN
α_T	−0.08	−1.57	2.37
δ_T	13.93	18.25	5.74

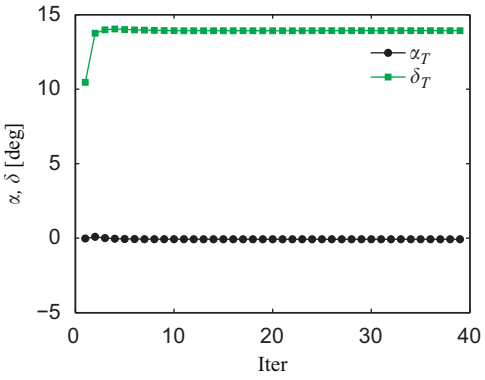

Fig. 11. Solution history.

7.2. Trim analysis

The trim condition for TCR case in simple symmetric cruise flight at MTOW, $M_{\infty}=0.65$, $z=0$ has been sought. As mentioned above, a subsonic flight regime has been considered in order to ease the validation process among the tools used. The methods have been applied for both the rigid and deformable case.

For the simple rigid case considered, the unknowns of the problem are represented by the angle of attack α and the deflection of the canard δ with a normal load factor $n_z=1$. The results are summarized in Table 18 and compared with those provided by SMARTCAD and MSC/NASTRAN. The values predicted by Edge and SMARTCAD relatively agree, considering the models are quite different. A small negative value of α and a relatively high canard deflection required to balance the aircraft are predicted. This would probably demand for improvements in the weight and balance process or in the initial aerodynamic layout design. Larger discrepancies are determined by MSC/NASTRAN which neglects in this case the built-in twist effects on the reference aerodynamic loading as showed above.

Of course, the differences in modeling show up when it concerns the trim solution. However SMARTCAD fairly agrees with the CFD solution, considering the fuselage is not modeled in terms of lift and interference contribution. Fig. 11 shows the history of the iterative trim process on α and δ for the CFD trim process. The initial reference condition is $\alpha=0$ and $\delta=0$. Being the problem basically linear, the prediction at the first iteration, based on the derivatives determined in correspond to this

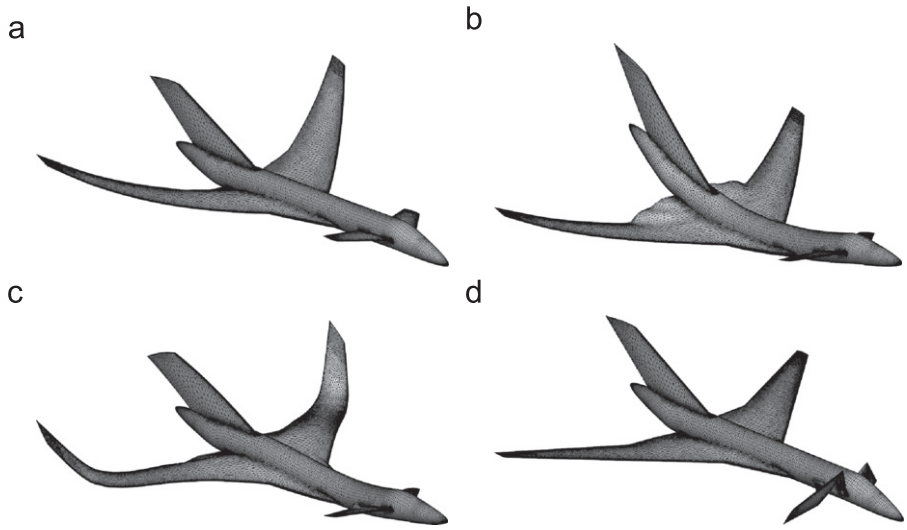

Fig. 12. Example of mode shapes considered for the aeroelastic trim: (a) Mode 7, (b) Mode 9, (c) Mode 16, (d) Canard rigid mode.

Table 19
Modal base adopted for the aeroelastic trim.

Mode	Freq. (Hz)	Description
7	1.85	First wing bending
9	2.48	Fuselage bending
12	3.36	In-plane wing bending
13	4.18	First torsional wing
16	6.44	Second wing bending
101	0.0	Rigid canard deflection

reference condition, is already close to the final result. In the following iterations indeed, only minor adjustments occur.

As for the deformable trim, the structural contribution is considered in two different ways: the full FE model is used for the low fidelity analysis with SMARTCAD while a modal approach is adopted for the CFD process. In this case, the modal base consists of the first five free–free vibration modes and the canard rigid deflection. Some of the considered modes are shown in Fig. 12 and briefly summarized in Table 19.

The history of the trim process is outlined in Fig. 13. After the first iterative loop on the fixed-shape trim problem, the trend is different compared to the one determined in the rigid process (see Fig. 11). The deflection of the canard is significantly affected by the effect of structural deformability on the lifting surfaces; a relatively small increase in α is required to compensate for their washout.

The convergence on the elastic problem, a part from the first six iterations, is fairly smooth and rapid. The first two vibration modes govern the structural response; the addition of further modes in the original modal base have turned out to add for negligible contributions to the final solution. After approximately ten iterations the problem has converged.

Fig. 14 shows the difference in the pressure coefficient distribution between the reference initial condition and the final one. The major difference occurs on the canard which again undergoes a relatively large deflection to compensate for the pitch moment. Fig. 15 shows the difference in pressure distribution between the trim solution for the rigid and deformable case along three different spanwise sections of the canard, respectively at a span fraction $\eta = 0.5$, 0.66 and 0.83. Since the deflection of the canard is lower than the rigid case, the overall aerodynamic load is reduced.

As for the wing, Fig. 16 highlights the aeroelastic effects along three different spanwise sections at $\eta = 0.44$, 0.67 and 0.89. The re-distribution for the aerodynamic load is clear. Because of aeroelastic effects and the washout occurring especially in the outboard sections, the spanwise resultant is shifted inboard. The trim solution for the elastic aircraft is compared with the results from linear theories available in SMARTCAD and MSC/NASTRAN. As reported in Table 20, α has to be increased and δ decreased when deformability is accounted for. SMARTCAD and Edge have a fairly good agreement for the trim parameters, while the solution provided by MSC/NASTRAN features larger discrepancies, being affected by the reference load which does not consider camber effects. The increase in α is approximately of 1° for all the methods adopted; SMARTCAD shows the largest variations in both α and δ. This implies the trimmed solution determined by SMARTCAD features higher differences in the re-distribution of the aerodynamic load compared to the rigid case. Such differences can be better highlighted considering the final deformed shape, briefly summarized in Table 20 in terms of the relative displacement Δs and deflection $\Delta\theta$ of the wing tip.

Considering again the solution provided by SMARTCAD, the tip features the lowest vertical displacement and highest twist deflection (the negative sign means here the local angle of attack is reduced). Thus, the aerodynamic resultant for the wing is moved inboard and hence upstream, implying a higher reduction in the canard deflection compared to the rigid case. As for the canard, no appreciable difference is highlighted.

7.2.1. *Aeroelastic derivatives*

In terms of aerodynamic derivatives, Table 21 reports the values for the longitudinal derivatives for the elastic aircraft at the flight condition considered, $q_\infty = 29\,645$ Pa. As for the solution predicted by Edge, the effects of the reference condition for the linearization point can be also included.

A different ROM has been indeed determined for each condition, i.e. $\alpha = 0$ or $\alpha = \alpha_T$. Also, the value of the steady derivatives with α can also be compared for a very low value of the reduced frequency k when a forced plunge motion is considered. The differences between the rigid and elastic cases can be better highlighted considering Table 22 which reports the correction coefficients η, defined as the ratio of the elastic and rigid values, i.e. $\eta(\cdot) = (\cdot)_E/(\cdot)_R$. All the three methods adopted have led to a good agreement for the corrections to CN_α and Cm_δ. This last

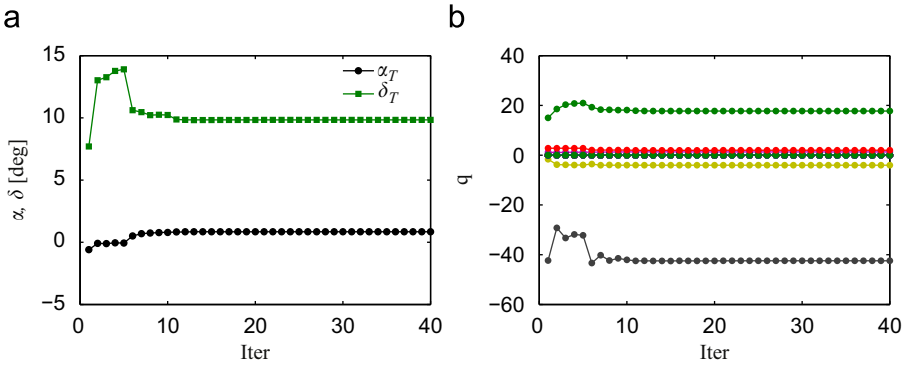

Fig. 13. Trim solution, $M_\infty = 0.65$, $z = 0$ m: (a) trim parameters, deformable and (b) modal amplitudes.

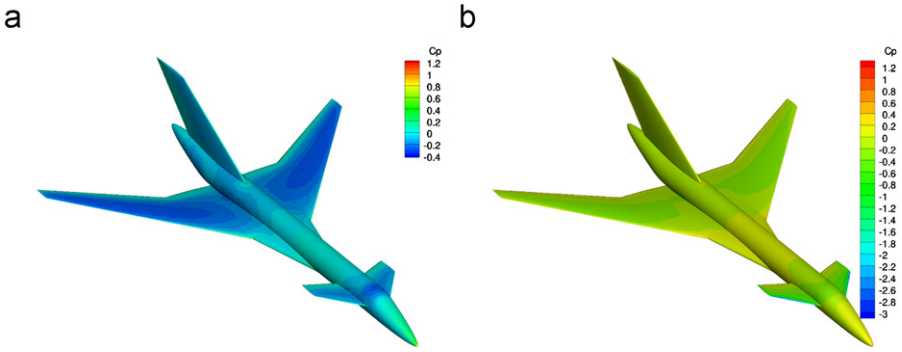

Fig. 14. Pressure coefficient contour for the reference and final deformed trimmed condition: (a) reference condition and (b) aeroelastic trim condition.

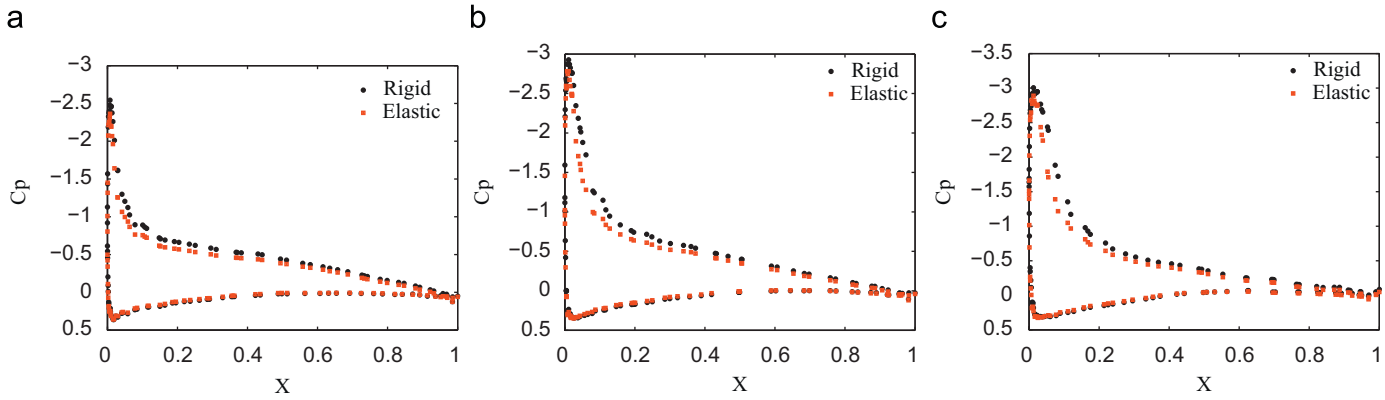

Fig. 15. Canard chordwise pressure coefficient, $M_\infty = 0.65$, $z = 0$ m: (a) $\eta = 0.50$, (b) $\eta = 0.66$ and (c) $\eta = 0.83$.

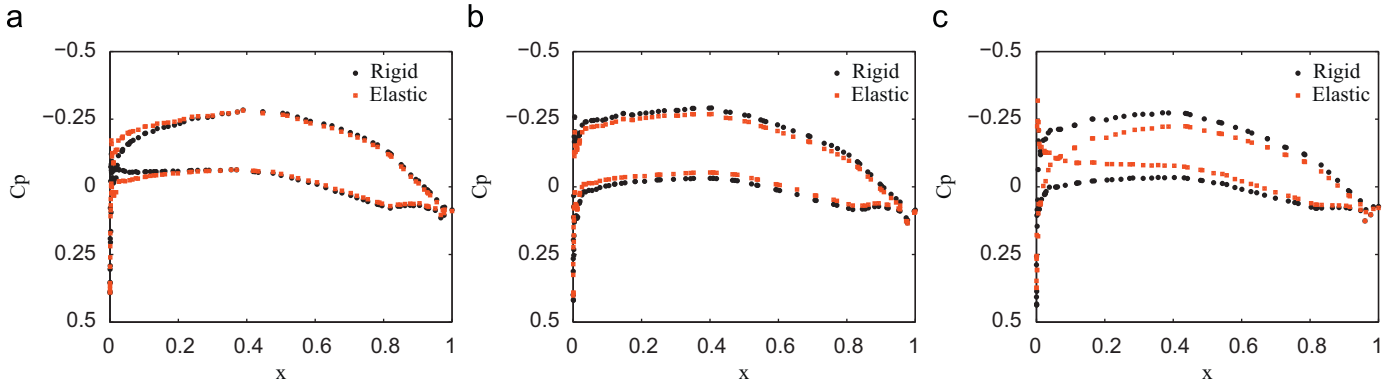

Fig. 16. Wing chordwise pressure coefficient, $M_\infty = 0.65$, $z = 0$ m: (a) $\eta = 0.44$, (b) $\eta = 0.67$ and (c) $\eta = 0.89$.

Table 20
Symmetric trim solution, $M_\infty = 0.65$, $z = 0$ m, deformable.

Trim values	Edge	SMARTCAD	MSC/NASTRAN
α_T	0.84	−0.17	3.53
δ_T	9.84	10.38	0.99
$\Delta s_{x,wtip}$	0.01	0.03	0.02
$\Delta s_{z,wtip}$	0.94	0.73	0.97
$\Delta s_{z,ctip}$	0.12	0.14	0.08
$\Delta\theta_{x,wtip}$	0.05	0.03	0.02
$\Delta\theta_{y,wtip}$	−0.05	−0.06	−0.07
$\Delta\theta_{x,ctip}$	0.00	0.013	0.00
$\Delta\theta_{y,ctip}$	0.01	−0.00	0.00

Table 21
Aeroelastic longitudinal steady derivatives, $M_\infty = 0.65$, $z = 0$ m, deformable.

Derivatives	Edge (ROM) $\alpha = 0$	Edge (ROM) $\alpha = \alpha_T$	SMARTCAD	MSC/NASTRAN
$\mathbf{CN}_\alpha$	2.86	2.85	2.80	2.51
$k = 0.01$	2.84	2.83		
$\mathbf{Cm}_\alpha$	−0.51	−0.36	0.15	−0.05
$k = 0.01$	−0.55	−0.42		
$\mathbf{CN}_\delta$	−0.05	−0.02	0.002	0.004
$\mathbf{Cm}_\delta$	0.53	0.62	0.36	0.39

Table 22
Aeroelastic correction to steady longitudinal derivatives, $M_\infty = 0.65$, $z = 0$ m, deformable.

Correction coefficients	Edge (ROM) $\alpha = \alpha_T$	SMARTCAD	MSC/NASTRAN
$\eta(\mathbf{CN}_\alpha)$	0.80	0.72	0.73
$\eta(\mathbf{Cm}_\alpha)$	0.31	−0.20	0.06
$\eta(\mathbf{CN}_\delta)$	−0.20	0.03	0.07
$\eta(\mathbf{Cm}_\delta)$	1.16	1.09	1.08

undergoes an increment mainly due to fuselage bending, confirmed by the different values predicted by Edge for the two ROMs.

The first difference to highlight relies in the Cm_α derivative which is significantly affected by deformability effects.

The solution predicted by MSC/NASTRAN almost reaches a null value, while SMARTCAD predicts even an inversion. On the other hand, the solution by Edge is still positive which probably highlights a beneficial effect from the fuselage. Finally, considering the derivative CN_δ the three solvers again agree on the general aeroelastic behavior for the aircraft considered. MSC/NASTRAN and SMARTCAD predict a coefficient tending to a null value, while for Edge the inversion has already occurred at this value of the dynamic pressure. This demands for a stiffening in fuselage bending. Indeed when mode n.9 is excluded from the modal base, the correction factor is still positive.

8. Conclusions

This work has presented a software environment for aero-structural conceptual design, named NeoCASS, which allows to design the airframe and study its aeroelastic behavior once the geometrical configuration is defined. NeoCASS is composed by different modules allowing the user to tackle all the aspects typical of aircraft conceptual design, starting from the initial weight and balance analysis, through the first structural sizing, till the final structural optimization. To include in the process a more rigorous physical approach, a specific module, named SMARTCAD aiming at the aeroelastic analysis and optimization, has been developed.

NeoCASS allows to consider the structural issue from the very beginning, improving the accuracy of the process which is necessarily iterative. In this respect the tool updates the current design with data such as airframe weight, overall weight and balance; the aerodynamic database is corrected with deformability effects and flight points are limited due to possible flutter instabilities. The tool allows to minimize the adoption of empirical formulas. The problem at hand is directly investigated through specific numerical methods. The computational costs are of course considered, given the high number of simulations to carried out and all the uncertainties typical of such an early phase. Thus, simple methods such as linear potential methods and stick models have been adopted. They represent a good compromise between accuracy and costs. Of course in some cases, such simplified approaches can lead to poor accuracy. Compressibility, viscous effects, aerodynamic interference can hardly be caught with such methods. Thus, tools of higher level of accuracy have to be adopted, such as CFD methods as showed in this paper. Of course this implies computational costs are raised. It is up to the designer to understand when the tools at hand can be trusted and used. As for structural models, currently a linear/non-linear beam elements is used to avoid recurring to solution, e.g. finite elements, requiring too much detail. These methods must be delegated to successive design steps in the preliminary phase. NeoCASS is integrated within a general design tool named CEASIOM, the outcome of the EU framework SimSAC. Each call to NeoCASS can be seen as an independent optimization loop for the final airframe within the overall optimization design process for the aircraft. The structural engineer can indeed drive a structural optimization process such that the airframe minimizes and undergoes different kinds of user-defined figures of merits. Most of the procedures developed are automated and easy to be carried out thanks to a user-friendly graphical interface.

After the synthesis of the capabilities offered by NeoCASS, a complete case study, regarding the target aircraft defined by SimSAC, has been reported. Three different levels of validation of the results obtained with NeoCASS have been reported, based on MSC/NASTRAN, a medium fidelity CFD tool and some available wind tunnel testing results, respectively. The adoption of enhanced tools shows the level of accuracy that can be reached when classic simplified methods are adopted.

Acknowledgements

Giampiero Bindolino and Paolo Mantegazza are acknowledged for the interesting discussions about Vortex Lattice Methods and the formulation of trim problems for linear aeroelasticity, while Andrea da Ronch for his initial contribution to the development of the GUESS module. A special thanks to Alessandro De Gaspari for the contribution to the GUI interface development and to Luca Riccobene for the implementation of W&B module. Alessandro Scotti is warmly acknowledged for his contribution to the TCR model design and manufacturing. The financial support by the European Commission through co-funding of the FP6 project SimSAC is acknowledged.

References

[1] Raymer DP. Aircraft design: a conceptual approach. 4th ed. New York, NY: AIAA Education Series; 2006.
[2] Torenbeek E. Synthesis of subsonic airplane design. Kluwer Academic Pub, Delft University Press; 1982.

[3] Lucia DJ. The sensorcraft configurations: A non-linear AeroServoElastic challenge for aviation. In: Proceedings of the 46th AIAA/ASME/ASCE/AHS/ASC SDM conference, Austin, Texas; 2005.
[4] Silva WA, Vartio E, Shimko A, Kvaternik RG, Eure KW, Scott R. Development of aeroservoelastic analytical models and gust load alleviation control laws of a sensorcraft wind-tunnel model using measured data. In: Proceedings of the IFASD international forum on aeroelasticity, Stockholm; 2007.
[5] Liebeck RH. Design of the blended wing body subsonic transport. Journal of Aircraft 2004;41(1):10–25.
[6] Antoine N, Kroo I, Willcox K, Barter G. A framework for aircraft conceptual design and environmental performance studies. In: Proceedings of the 10th AIAA/ISSMO multidisciplinary analysis and optimization conference, Albany, New York; 2004.
[7] Macci SH. Semi-analytical method for predicting wing structural mass. Technical Report, SAWE Paper No. 2282; 1995.
[8] Bindolino G, Ghiringhelli G, Ricci S. Multilevel structural optimization for preliminary wing-box weight estimation. Journal of Aircraft 2010;47(2):475–89.
[9] Ardema M, Chambers A, Hahn A, Miura H, Moore M. Analytical fuselage and wing weight estimation of transport aircraft. Technical Report 110392. NASA, Ames Research Center, Moffett Field, California; 1996.
[10] Cavagna L, Ricci S, Riccobene L. A fast tool for structural sizing, aeroelastic analysis and optimization in aircraft conceptual design. In: Fiftieth AIAA/ASME/ASCE/AHS/ASC structures, structural dynamics and materials conference. Palm Springs, California; 2009.
[11] Cavagna L, Ricci S, Travaglini L. Aeroelastic analysis and optimization at conceptual design level using NeoCASS suite. In: Fifty-second AIAA/ASME/ASCE/AHS/ASC Structures, Structural Dynamics and Materials Conference. Denver, Colorado; 2011.
[12] Mason WH. 〈http://www.aoe.vt.edu/~mason/Mason_f/MRsoft.html/〉, LDSTAB software [last accessed 2009].
[13] Shanley FR. Weight-strength analysis of aircraft structures. 2nd ed. New York: Dover Publications, Inc.; 1960.
[14] Crawford RF, Burns AB. Minimum weight potentials for stiffened plates and shells. AIAA Journal 1963;1(4):879–86.
[15] Moran J. An introduction to theoretical and computational aerodynamics. John Wiley & Sons; 1984.
[16] Katz J, Plotkin A. Low-speed aerodynamics from wing theory to panel methods. McGraw-Hill Series in Aeronautical and Aerospace Engineering; 1991.
[17] Albano E, Rodden WP. A doublet–lattice method for calculating the lift distributions on oscillating surfaces in subsonic flow. AIAA Journal 1969;7(2):279–85.
[18] Chen PC, Liu DD. A harmonic gradient method for unsteady supersonic flow calculations. Journal of Aircraft 1985;22(15):371–9.
[19] Ghiringhelli GL, Masarati P, Mantegazza P. A multi-body implementation of finite volume beams. AIAA Journal 2000;38(1):131–8.
[20] Quaranta G, Masarati P, Mantegazza P. A conservative mesh-free approach for fluid-structure interface problems. In: Papadrakakis M, Oñate E, Schrefler B, editors. International conference on computational methods for coupled problems in science and engineering. Santorini, Greece: CIMNE; 2005.
[21] Beckert A, Wendland H. Multivariate interpolation for fluid-structure-interaction problems using radial basis functions. Aerospace Science Technology 2001;5:125–34.
[22] Haftka RT, Gürdal Z. Elements of structural optimization.3rd ed. Dordrecht: KLUWER; 1992. [ISBN 0-7923-1504-9].
[23] Attorni A, Cavagna L, Quaranta G. Aircraft T-tail flutter prediction using computational fluid dynamics. Journal of Fluids and Structures 2011;27(2):161–74.
[24] Cavagna L, Masarati P, Quaranta G. Coupled multibody/computational fluid dynamics simulation of maneuvering flexible aircraft. Journal of Aircraft 2011;48(1):92–106.
[25] Rodden W, Love J. Equations of motion of a quasisteady flight vehicle utilizing restrained static aeroelastic characteristics. Journal of Aircraft 1985;22(3):802–9.
[26] Fisher C, Arena A. On the transpiration method for efficient aeroelastic analysis using an Euler solver. In: Proceedings of the AIAA atmospheric flight mechanics conference. San Diego, CA; 1996.
[27] Cavagna L, Quaranta G, Mantegazza P. Application of Navier–Stokes simulations for aeroelastic assessment in transonic regime. Computers & Structures 2007;85(11–14):818–32. [Fourth MIT conference on computational fluid and solid mechanics].
[28] Rodden W, Gesling J. Application of oscillatory aerodynamic theory to estimation of stability derivatives. Journal of Aircraft 1970;7(3):272–5.